Published in final edited form as:
J Comp Neurol. 2006 October 20; 498(6): 786–795.

Differences in Chemo- and Cytoarchitectural Features within *Pars Principalis* of the Rat Anterior Olfactory Nucleus Suggest Functional Specialization

ELIZABETH AMORY MEYER[1], **KURT R. ILLIG**[2], and **PETER C. BRUNJES**[2,*]
1*Department of Biology, University of Virginia, Charlottesville, Virginia, 22904*

2*Department of Psychology, University of Virginia, Charlottesville, Virginia, 22904*

Abstract

The anterior olfactory nucleus (AON) lies between the olfactory bulb and piriform cortex and is the first bilaterally innervated structure in the olfactory system. It is typically divided into two subregions: *pars externa* and *pars principalis*. We examined the cytoarchitecture of *pars principalis*, the largest cellular area of the region, to determine whether it is homogeneously organized. Quantitative Nissl studies indicated that large cells (cell body area >2 standard deviations (SD) larger than the mean cell size) are densest in lateral and dorsolateral regions, while small cells (>1 SD smaller than the mean) are more numerous in medial and ventral areas. Further evidence for regional differences in the organization of the AON were obtained with immunohistochemistry for calbindin (CALB), parvalbumin (PARV), glutamic acid decarboxylase (GAD), and choline transporter (CHT). Cells immunopositive for CALB (CALB+) were denser in the deep portion of Layer II, although homogeneously dispersed throughout the circumference of the AON. PARV+ cells were located in the superficial half of Layer II and were sparse in ventral and medial regions. CHT+ and GAD+ fibers were denser in lateral versus medial regions. No regional differences were found in GAD+ somata, or in norepinephrine transporter or serotonin transporter immunoreactivity. The observed regional differences in cyto- and chemoarchitectural features may reflect functional heterogeneity within the AON.

Keywords

olfactory cortex; olfactory system organization; olfactory peduncle

Olfactory stimuli enter the nasal cavity and activate olfactory sensory neurons which transmit the information to the olfactory bulb. After processing in the bulb, the signal is sent to the anterior olfactory nucleus (AON) and piriform cortex via the lateral olfactory tract (Fig. 1A). The AON, found caudal to the olfactory bulb and rostral to the piriform cortex, is the main component of the olfactory peduncle and is the first structure in the olfactory pathway to have bilateral connections: it has bidirectional interactions with the contralateral AON, olfactory bulb, and piriform cortex via the anterior commissure. Although relatively large, very little is known about the cytoarchitecture or function of the AON (see Brunjes et al., 2005, for a review).

Historically, the AON has been divided into two subregions, *pars externa* (a thin ring of cells found at the junction of the bulb and AON), and "*pars principalis*," a two-layered structure

*Correspondence to: P.C. Brunjes, 102 Gilmer Hall, PO Box 400400, Charlottesville, VA 22904-4400. E-mail: brunjes@virginia.edu
Grant sponsor: National Institutes of Health; Grant number: NIH DC0338; Grant number: NIH DC005557.

consisting of an outer plexiform layer (Layer I) and an inner broad ring of cells (Layer II; Fig. 1B; Brunjes et al., 2005). *Pars principalis* has often been divided into four regions based on geography: *pars medialis, pars dorsalis, pars lateralis*, and *pars ventroposterior*. However, the literature reveals a wide discrepancy in the definitions of these areas (see fig. 4 in Brunjes et al., 2005). Nevertheless, several indications suggest that *pars principalis* consists of functionally distinct subdivisions. For example, the medial side of the region contains relatively small, tightly packed cells (Haberly and Price, 1978) and has substantially different afferent and efferent fiber systems (e.g., Haberly, 2001;Neville and Haberly, 2004). Further, Haberly (2001) noted that the dorsal, lateral, and ventral regions receive direct input from the lateral olfactory tract and transmit it to the piriform cortices, while the medial zone does not. These and other indications of differential innervation from both within the olfactory system and from other brain regions indicate that the region is complex (see Brunjes et al., 2005). The studies presented below begin to quantify the cytoarchitectural and neurochemical features of *pars principalis* to determine if it can be further differentiated on an anatomical basis.

MATERIALS AND METHODS

Animals and tissue preparation

Male (~250-350 gm; Long Evans; Harlan, Indianapolis, IN) rats were used and all procedures were performed according to NIH guidelines and protocols approved by the University of Virginia IACUC. Animals were housed in standard polypropylene cages with food (Harlan Rat Chow 8604) and water ad libitum. The colony was maintained on a 12:12 light:dark cycle in a temperature-controlled room (22°C). Animals were given a lethal injection of euthanasia solution (Euthasol, 1 mL/250 g injection volume) and perfused transcardially with 0.01 M phosphate-buffered saline (pH 7.4, PBS) containing heparin followed by 4% buffered paraformaldehyde (for Nissl, calbindin (CALB), parvalbumin (PARV), glutamic acid decarboxylase (GAD) without Triton (TX; GAD-TX), GAD/CALB and GAD/PARV double labeling studies, see below) or 4% paraformaldehyde containing 15% picric acid (for serotonin transporter (SERT), norepinephrine transporter (NET), choline transporter (CHT), and GAD +TX studies). Tissue for the Nissl study was embedded in glycol methacrylate (JB-4+; Polysciences, Warrington, PA) and serial 2 μm-thick coronal sections cut with carbide knives were stained with Toluidine blue O. For all other studies, brains were removed and postfixed for ~4 hours and then cryoprotected in 30% sucrose/PBS. The following day, 50-μm sections were cut on a cryostat. Every second section was taken for immunohistochemical processing and analysis.

Nissl study

For each of the three animals used, three sections were selected from the region of the AON near the caudal remnant of the granule cell layer of the olfactory bulb. The three sections were separated by at least 100 μm. A composite image of each section was made with a 60× objective using the tiled field map routine of an image analysis software package (MCID 7.0 Elite; Interfocus Imaging, Linton, UK). Neurons were defined as large profiles containing a clear nucleus. For each neuron, the XY coordinates, soma area, and shape factor (ratio of long and short axes) was recorded. In order to align sections, polar plots were then created from the X and Y coordinates. Regional variations in cell size and shape were examined by determining which cells were 2 SD or more above mean cell size and those more than 1 SD below the mean.

Immunostaining procedure

GAD. As a marker for GABAergic cells and fibers, immunohistochemistry for GAD-67 was run with and without TX (Ekstrand et al., 2001) to visualize boutons and cartridges and/or cell bodies, respectively. Standard fluorescent immunostaining was used to stain tissue from four animals. Briefly, sections were rinsed twice in 0.01 M PBS, incubated in 0.3% H_2O_2 for 30

minutes at room temperature, then rinsed three times for 10 minutes each in a wash buffer containing 0.01 M PBS with 1% bovine serum albumin (BSA) alone or with 0.5% TX. Sections were then incubated in a blocking buffer that contained 0.01 M PBS, 1% BSA alone, or with 0.5% TX and 20% normal goat serum (NGS). The tissue was subsequently labeled with primary antibody (rabbit anti-glutamate decarboxylase (GAD) polyclonal antibody, 1:1,000, AB5992, Lot 24030212, Chemicon, Temecula, CA) in wash buffer containing 2% NGS via incubation of sections overnight on a shaker at room temperature. The immunogen for the GAD antibody was a recombinant fusion protein containing the unique N-terminal region of GAD-67 that is not shared by GAD-65. Western blots reveal that the GAD antibody predominantly recognizes the larger form of GAD (67 kD), with some reactivity to GAD65 (manufacturer's technical information). Immunostaining with the GAD67 antibody colocalizes with staining with antibodies directed against GABA (Heinke et al., 2004). Additionally, the GAD67 antibody specificity has been verified by incubating tissue with antibody solution preabsorbed with purified GAD67 protein (Horn et al., 1998). The following morning, sections were rinsed 6 × 10 minutes in wash buffer (again, with or without TX) and incubated in fluorescent secondary antibody (1:500, Alexa-Fluor 488 goat antirabbit IgG; Molecular Probes, Eugene, OR) in wash buffer containing 0.5% BSA and 2% NGS at room temperature, in the dark for 3 hours. Sections were then rinsed in the dark in PBS. For those sections treated with TX, brief staining with a fluorescent Nissl marker occurred following secondary incubation and sections were then rinsed with PBS three times. For all immunohistochemistry, sections processed without the addition of primary antibodies were used as controls for the specificity of the secondary antiserum.

CALB and PARV. Standard immunohistochemistry was used to stain free-floating sections from five animals for each of these calcium-binding proteins. Briefly, sections were rinsed three times in a 0.1 M phosphate buffer (PB) wash buffer containing 0.5% TX and 2% BSA. Next, sections were incubated for 30 minutes at room temperature in 0.3% H_2O_2, rinsed three times in wash buffer, then incubated in blocking serum made up of 0.5% TX, 20% NGS, and 2% BSA in 0.1 M PB. Tissue was then incubated overnight at room temperature in primary antibodies raised in mouse (monoclonal anti-calbindin-D-28k clone CB-955, 1:25,000, Sigma, St. Louis, MO, C9848, Lot 113K4867, or monoclonal anti-parvalbumin clone PARV-19, 1:500, Sigma P3088, Lot 033K4846) made up in wash buffer containing 1% NGS. The following day, sections were rinsed four times in wash buffer then incubated for 3 hours at room temperature in secondary antibody (biotinylated antimouse, 1:500, Vector, Burlingame, CA). Mono-clonal anti-calbindin-D-28K antibody is derived from the CB-955 hybridoma produced by the fusion of mouse myeloma cells and splenocytes from BALB/c mice immunized with purified bovine kidney calbindin-D-28k. Immunoblotting revealed that the antibody recognizes the calbindin-D-28k band (manufacturer's technical information). Monoclonal anti-parvalbumin antibody (mouse IgG1) is derived from the PARV-19 hybridoma produced by the fusion of mouse mylenoma cells and splenocytes from a mouse immunized against purified frog muscle parvalbumin. Immunoblotting revealed that the parval-bumin antibody recognizes the 12 kD form of parvalbumin (manufacturer's technical information). Following secondary incubation, sections were rinsed four times in wash buffer and incubated in Avidin-Biotin Complex for 1 hour at room temperature. Finally, sections were rinsed and stained with DAB. Sections through the AON revealed labeled cells with the same morphology and patterns of distribution as calbindin and parvalbumin staining seen in previous studies (e.g., Garcia-Ojeda et al., 1992; Ohm, Müller and Braak, 1991; Barbado et al., 2002).

GAD double with CALB/PARV. Double-labeling fluorescent immunohistochemistry was used to visualize the presence of GAD with CALB and PARV. The same procedure as stated above for GAD-TX was employed.

CALB/PARV double labeling. The same standard fluorescent immunohistochemistry described above for CALB/PARV and GAD-TX staining was used to doublestain sections for CALB and PARV (anti-calbindin-D-28K antibody raised in rabbit, Sigma, C2724, Lot 035K4765, and monoclonal anti-parvalbumin clone PARV-19, 1:500, Sigma P3088). The immunogen used for Anti-Calbindin D-28K (EG20) antibody produced in rabbit was the synthetic peptide corresponding to the C-terminal region of rat calbindin-D-28K (amino acids 225-244 with N-terminally added Lys-Gly) conjugated to KLH. By immunoblotting, staining of calbindin-D-28k is specifically inhibited with the calbindin-D-28K immunizing peptide. Western blots reveal that this antibody reacts with a single band of ~28 kDa (Ecay et al., 2004). This antibody produced staining similar to that seen with the monoclonal calbindin antibody mentioned above.

NET, SERT, and CHT. Fluorescent immunohistochemistry was used to stain free-floating tissue from seven animals for each transporter. Briefly, sections were rinsed twice in 0.01 M PBS, incubated in 0.3% H_2O_2 for 30 minutes at room temperature, then rinsed three times for 10 minutes each in a wash buffer containing 0.01 M PBS with 1% BSA and 0.5% TX. Sections were then incubated in a blocking buffer that contained 0.01 M PBS, 1% BSA, 0.5% TX, and 10% NGS. The tissue was subsequently labeled with primary antibody (1:1,000; rabbit antirat norepinephrine transporter affinity purified polyclonal antibody (Chemicon AB5066P, Lot 24040502), 1:2,500, mouse anti-serotonin transporter monoclonal antibody (Chemicon MAB1564), 1:2,500, rabbit anti-choline transporter, high affinity polyclonal antibody (Chemicon AB5966, Lot 25030004)) in wash buffer + 2% NGS via incubation of sections overnight on a shaker at room temperature. The NET antibody recognizes the 22 amino acid peptide sequence mapping to the first extracellular domain of rat NET (manufacturer's technical information). This NET antiserum stains a single band of 80 kD molecular weight on a Western blot (Kantor et al., 2001). Additionally, no staining was seen when the NET antiserum was used to stain tissue in an NET knockout mouse (Mundorf et al., 2001). The SERT antibody immunogen was the rat serotonin transporter, N-terminus/GST fusion protein (amino acids 1-85). Western blots reveal that the monoclonal SERT antibody binds specifically to the aforementioned fusion protein and control tissue showed no SERT staining with incubation with preimmune sera (Schroeter et al., 1997; Brown and Molliver, 2000). The CHT antibody reacts to the 70 kDa protein in the mouse spinal cord and a doublet of the 70-75 kDa in mouse striatal tissue homogenates in a Western blot (manufacturer's technical information). The immunogen for the CHT antibody was the human CHT fusion protein. The CHT antiserum has been shown to mark cholinergic fibers that match staining in other systems (Bergeron et al., 2005). Additionally, levels of immunoreactivity with the CHT antibody correspond to mRNA levels in CHT knockdown mice (Brandon et al., 2004).

The following morning, sections were rinsed 6 × 10 minutes in wash buffer and incubated in fluorescent secondary antibody (all 1:500; Alexa Fluor; Molecular Probes) at room temperature in the dark for 3 hours. Sections were then rinsed in the dark in PBS, briefly stained with a fluorescent Nissl stain (Sytox, Molecular Probes), and rinsed again three times with PBS.

Acquisition and quantification of immunostained tissue

An Olympus Fluoview confocal microscope was used to obtain stacks of images of the fluorescently labeled tissue. Five areas were chosen for analysis (Figs. 1B, 2A) and images acquired from each in a random order. The method allowed an overview of several standardized regions of the AON while avoiding photobleaching. For SERT and NET tissue, images were made with a 20× or 40× objective, respectively. A suitable region was chosen and the microscope centered in the middle of the section. Ten images were obtained, each 1 μm thick, and separated by 1 μm. Each focal plane was scanned four times and the results averaged. Subsequently the 10 images were combined. Ten GAD-TX, GAD+TX, GAD/CALB, GAD/

PARV, CALB/PARV, and CHT images were taken by averaging four scans at 40× (for, GAD/CALB, GAD/PARV, and CALB/PARV) or 10 images at 20× (for GAD-TX and GAD+TX).

For NET, SERT, CHT, GAD-TX, and GAD +TX stained tissue, each composite image was loaded into the image analysis program and the density of labeled fibers in five regions of the central-most region of the AON (Fig. 1B) was quantified. Staining thresholds were standardized using the MCID image analysis system. The proportion of test area (100 x 150 μm^2 box for 20x images and 100x300μm^2 box for 40x images) that exhibited immunostaining was recorded for each position and subjected to statistical analyses.

Tissue stained with DAB for CALB and PARV antibodies was analyzed by creating a tiled field map using same process outlined above (with a 20× objective). Layer II of *pars principalis* was divided into eight equal bins based on cardinal points (Fig. 2F). Each bin was also subdivided into superficial and deep halves and the numbers of calbindin- and parvalbumin-immunoreactive cells were recorded. Adobe Photoshop (San Jose, CA) was used to crop photomicrographs and adjust brightness and contrast in order to produce the plates.

RESULTS

Distribution of Nissl-stained cells

The nine sections examined yielded a sample of 15,960 cells. Figure 1C is a composite showing the cells in matched anterior sections from each of three animals. This polar plot indicates that the profiles were distributed relatively homogeneously throughout Layer II. An analysis of cell size (profile area) yielded a unimodal distribution, with a mean area of 84.75 μm^2 (range: ~20 to ~200 μm^2; Fig. 1D). However, a closer analysis revealed that cells of different sizes were differentially distributed throughout the AON. Large cells (i.e., more than 2 SD larger than mean cell size) were preferentially located in dorsolateral regions (Fig. 1E), whereas small cells (more than 1 SD smaller the mean cell size) were found in the ventromedial portions of the AON (Fig. 1F). An analysis of cell shape data (the ratio of long to short axis) revealed that most cells were spherical (Fig. 1G). No regional differences in the distribution of round- or flat-shaped cells were found (Fig. 1H).

Distribution of GABAergic cells

The striking differences in tissue organization (depicted in Fig. 1E,F) suggested that the ventral and medial regions of *pars principalis* might contain substantial numbers of interneurons. Therefore, the distribution of GABAergic cell bodies was examined using an antibody to GAD-67. A large number of cells immunoreactive for the antigen were found throughout the AON (Fig. 2B). No regional differences in number of GAD-67-positive cell bodies were encountered (analysis of variance (ANOVA), $F_{(4,54)} = 0.911$, $P > 0.05$; Fig. 2C).

To determine if there were any regional patterns in the expression of specific subpopulations of GABAergic neurons, the distribution of cells expressing the calcium- binding proteins CALB and PARV were examined. Double-label staining indicated that cells expressing each of these calcium-binding proteins were also GABAergic; most CALB- and PARV-positive cells were double-labeled with GAD (Fig. 2D,E). Relatively little overlap was seen in tissue double-labeled for PARV and CALB (Fig. 2E).

Each subpopulation of cells was concentrated in different regions of *pars principalis*. CALB-positive cells were significantly more prevalent in the deep portion of Layer II (ANOVA $F_{(1,64)} = 45.176$ $P < 0.05$; Fig. 2G-I). Despite this laminar difference, CALB-positive cells were distributed homogeneously throughout the circumference of *pars principalis* (ANOVA $F_{(7,64)} = 1.735$, $P > 0.05$, Fig. 2G-I). There was a significant interaction between the radial location of the cells and deep versus superficial labeling (ANOVA $F_{(7,64)} = 3.708$, $P < 0.05$,

Fig. 2I), and post-hoc tests revealed significantly more CALB cells in the deep layers in bins 4, 5, 6, 7, and 8 (Bonferroni corrected *t*-test; $P < 0.05$ for each, Fig. 2I). Thus, CALB+ cells are more prevalent in deep layers of the lateral portion of the AON. Cells immunoreactive for PARV displayed a different distribution than CALB-positive cells (Fig. 2J-L). First, significantly more PARV-positive cell bodies were found in the dorsolateral portion of the AON (i.e., bins 4-7), and were relatively absent from the ventral and medial portions (i.e., positions 1, 2, and 8; ANOVA $F_{(7,64)} = 17.180$, $P < 0.05$; post-hoc tests with Tukey's HSD, $P < 0.05$ for each, Fig. 2L). Further, PARV-positive cells were significantly more abundant in the superficial layer than in the deep layer of *pars principalis* (ANOVA $F_{(1,64)} = 11.553$, $P < 0.05$, Fig. 2L).

Distribution of GABAergic terminals

To further study GABAergic processing in the AON, the distribution of GAD-immunoreactive processes and terminals in Layer II was examined (Fig. 3A,B). Labeled fibers were heterogeneously distributed within the AON, with a significantly higher density in the lateral portion (position 4) of *pars principalis* than in the medial (position 1), ventral (position 5) and dorsal (position 2) portions (ANOVA $F_{(4,43)} = 7.175$, $P<0.001$; post-hoc analyses with Tukey's HSD; $P < 0.05$ for each, Fig. 3G).

Distribution of centrifugal afferents

Regional differences in organization might be reflected in differential innervation by monoamine and other general regulatory inputs (Fig. 3C-G). CHT-labeled fibers were denser in the lateral (position 4, Fig. 3D) than in the medial (position 1, Fig. 3C) region of *pars principalis* (main effect of position; $F_{(4,89)} = 2.725$, $P < 0.05$; Tukey's HSD, $P < 0.05$, Fig. 3G). Although no significant differences were found for any comparisons among positions 1 through 5 for SERT (Fig. 3E,G) or NET (Fig. 3F,G), each revealed a similar trend, with position 4 having the densest immunoreactivity (Fig. 3G).

DISCUSSION

As outlined above (also see Brunjes et al., 2005), the primary cellular region of the AON ("*pars principalis*") is often arbitrarily subdivided using geographical landmarks or other subjective criteria. The experiments in this study were designed to examine the possibility that the AON has regional differences in anatomical organization. The heterogeneous distribution of several features, including variations in cell size and shape and the distribution of various chemically defined projections, indicate that the zone is not uniform (Fig. 4). These results support a role for the AON that is substantially more complex than has been previously thought. Each of these findings is discussed in more detail below.

Cell morphology

The first approach was to examine the shape, size, and location of almost 16,000 neuronal somata in Nissl-stained thin sections from three animals. Although no regional differences with respect to cell shape (ratio of major to minor axis) were observed, a differential distribution on the basis of cell size was encountered. Large cells were found in the dorsolateral portion of the AON, whereas smaller cells were preferentially located in the ventromedial portion. The findings suggest that there are regional differences in organization and function. In many brain regions, large cell bodies are indicative of longer projecting neurons (e.g., the giant pyramidal or "Betz" cells of the motor cortex project well into the spinal cord; mitral cells of the olfactory bulb have projections to the entorhinal cortex), while smaller cells are generally interneurons. One plausible conclusion, therefore, is that the dorsolateral regions of *pars principalis* would contain the longest projecting neurons, while the ventromedial aspect would have the highest density of locally projecting cells. The finding of smaller cells on the medial side is consistent

with Haberly and Price (1978), who used a similar observation to define "*pars medialis*." Also consistent with these observations is the finding that neurons in the medial and ventroposterior regions project heavily within the ipsilateral AON (Haberly and Price, 1978;Luskin and Price, 1983; also see review, Brunjes et al., 2005), while dorsal and lateral neurons project as far as periamygdaloid cortex (Lohman, 1963).

GABAergic cells

Since many small cells are GABAergic interneurons, the next set of studies examined the distribution of cells expressing GAD in *pars principalis*. GAD-67-immunocytochemistry revealed that *pars principalis* contains a substantial number of uniformly distributed cells with this phenotype. It has been well established in the piriform cortex and other regions that there are many sub- species of GABAergic cells that coexpress other neurotransmitters such as CALB and PARV (Celio, 1986; Jones and Hendry, 1986; Kosaka et al., 1987, 1995; DeFelipe et al., 1989a,1989b;Hendry et al., 1989; Kubota and Jones, 1993; Kubota et al., 1994; Ekstrand et al., 2001; McDonald and Mascagni, 2001; Kawaguchi and Kondo, 2002), therefore the distribution of cells expressing these calcium-binding proteins was explored (Garcia-Ojeda et al., 1992). Both were found to colocalize with GAD in the AON, but were only infrequently found to co-occur. Interesting regional differences in the distribution of CALB and PARV were observed. For example, PARV-immunostained cell bodies were found primarily in the superficial half of Layer II in the dorsolateral portion of *pars principalis*. Staining was almost absent in the ventral and medial portion of the AON. These findings mirror those from the Nissl data in that they suggest that there are medial/lateral differences within *pars principalis*. In contrast, CALB-staining pre- dominated in the deeper portion of Layer II, indicating that another potential axis of organization in the region is along the deep-superficial axis. Examination of GAD-positive fibers and boutons also revealed regional organization, with the highest density of processes in lateral regions (Fig. 3A,B,G). Taken together, these features suggest that GABAergic function is 1) widely spread throughout the AON on the basis of the uniform distribution of cell bodies, 2) particularly important in lateral regions, on the basis of the density of fibers, and 3) is mediated by several different regional subsystems, as suggested by the observed differences in cells expressing CALB and PARV.

Neuromodulatory inputs. The previous findings prompted an examination of the cholinergic, serotonergic, and noradrenergic innervation of the region with the rationale that if indeed there is differential function it might be mirrored in variations in the patterns of these general regulators. Indeed, large differences in these inputs characterize other regions such as the cortex, where they seem to delineate functionally different domains (e.g., DeFelipe, 1993; DeFelipe et al., 2002; Kimura, 2002; Job and Tan, 2003; Douglas et al., 2004; Benavides-Piccione et al., 2005). Regionally distinct patterns were observed in cholinergic input, with substantially more CHT staining in lateral than medial areas (Fig. 3C,D,G). Interestingly, these results mirror the findings for GAD fibers described above. While no statistically significant differences were observed for SERT or NET, they too exhibited highest staining densities in the lateral location. Therefore, it is quite likely that *pars principalis* is differentially influenced by the activation of these general arousal mechanisms, once again reaffirming regional differences in its function.

CONCLUSIONS

The data presented above suggest that the central cellular zone of the AON is more complicated than has previously been appreciated. Using quantitative methods, we have described several regional differences in the zone's cellular and neurochemical organization that suggest both radial and deep-to-superficial organization (see Fig. 4). Interestingly, some of these differences map well with Haberly's (2001; see also Brunjes et al., 2005) suggestion that the medial portion of the AON processes different information than the lateral side. These findings represent an

important first step into understanding the central role that the AON plays in olfactory information processing.

LITERATURE CITED

Barbado MV, Brinon JG, Weruga E, Porteros A, Aijon J, Alonso JR. Changes in immunoreactivity to calcium-binding proteins in the anterior olfactory nucleus of the rat after neonatal olfactory deprivation. Exp Neurol 2002;177:133–150. [PubMed: 12429217]

Benavides-Piccione R, Arellano JI, DeFelipe J. Catecholaminergic innervation of pyramidal neurons in the human temporal cortex. Cereb Cortex 2005;15:1584–1591. [PubMed: 15703259]

Bergeron AL, Schrader A, Yang D, Osman AA, Simmons DD. The final stage of cholinergic differentiation occurs below inner hair cells during development of rodent chochlea. J Assoc Res Otol 2005;6:401–415.

Brandon EP, Mellot T, Pizzo DP, Coufal N, D'Amour KA, Gobeske K, Lortie M, Lopez-Coviella, Berse B, Thal LJ, Gage FH, Blusztajn JK. Choline transporter 1 maintains cholinergic function in choline acetyltransferase haploinsufficiency. J Neurosci 2004;24:5459–5466. [PubMed: 15201317]

Brown P, Molliver ME. Dual serotonin (5-HT) projections to the nucleus accumbens core and shell: relation of the 5-HT transporter to amphetamine-induced neurotoxicity. J Neurosci 2000;20:1952–1963. [PubMed: 10684896]

Brunjes PC, Illig KR, Meyer EA. A field guide to the anterior olfactory nucleus/cortex. Brain Res Rev 2005;50:305–335. [PubMed: 16229895]

Celio MR. Parvalbumin in most γ-aminobutyric acid-containing neurons of the rat cerebral cortex. Science 1986;231:995–997. [PubMed: 3945815]

DeFelipe J. Neocortical neuronal diversity: chemical heterogeneity revealed by colocalization studies of classical neurotransmitters, neuropeptides, calcium binding proteins, and cell surface molecules. Cereb Cortex 1993;3:273–289. [PubMed: 8104567]

DeFelipe J, Hendry SHC, Jones EG. Synapses of double bouquet cells in monkey cerebral cortex visualized by calbindin immunoreactivity. Brain Res 1989a;400:303–317.

DeFelipe J, Hendry SHC, Jones EG. Visualization of chandelier cell axons by parvalbumin immunoreactivity in monkey cerebral cortex. Proc Natl Acad SciUSA 1989b;86:2093–2097.

DeFelipe J, Alonso-Naclares L, Arellano JI. Microstructure of the neocortex: comparative aspects. J Neurocytol 2002;31:299–316. [PubMed: 12815249]

Douglas, R.; Markham, H.; Martin, K. The synaptic organization of the brain. 5th ed.. Oxford University Press; New York: 2004. Neocortex; p. 499-558.

Ecay TW, Stewart JR, Blackburn DG. Expression of calbindin-D28k by yolk sac and chorioallatoic membranes of the corn snake, *Elaphe guttata*. J Exp Zool (Mol Dev Evol) 2004;302B:517–525.

Ekstrand JJ, Domroese ME, Johnson DMG, Feig SL, Knodel SM, Beiian M, Haberly LB. A new subdivision of the anterior piriform cortex and associated deep nucleus with novel features of interest for olfaction and epilepsy. J Comp Neurol 2001;434:289–307. [PubMed: 11331530]

Garcia-Ojeda E, Alonso JR, Arevalo R, Brinon JG, Lara J, Aijon J. Distribution of calbindin D-28K and parvalbumin immunoreactivities in the nucleus olfactorius anterior of the rat. Brain Res Bull 1992;29:783–793. [PubMed: 1473012]

Haberly LB. Parallel-distributed processing in olfactory cortex: new insights from morphological and physiological analysis of neuronal circuitry. Chem Senses 2001;26:551–576. [PubMed: 11418502]

Haberly LB, Price JL. Association of commissural fiber systems of the olfactory cortex of the rat. II. Systems originating in the olfactory peduncle. J Comp Neurol 1978;178:781–808.

Heinke B, Ruscheweyh R, Forsthuber L, Wunderbaldinger G, Sandkuhler J. Physiological, neurochemical and morphological properties of a subgroup of GABAergic spinal lamina II neurons identified by expression of green fluorescent protein in mice. J Physiol 2004;560.1:249–266. [PubMed: 15284347]

Hendry SHC, Jones EG, Emson PC, Lawson DEM, Heizman CW, Streit P. Two classes of GABA neurons defined by differential calcium binding protein immunoreactivities. Exp Brain Res 1989;76:467–472. [PubMed: 2767197]

Horn EM, Shonis CA, Holzwarth MA, Waldrop TG. Decrease in glutamic acid decarboxylase level in the hypothalamus of spontaneously hypertensive rats. J Hypotens 1998;16:625–633.

Job C, Tab S. Constructing the mammalian neocortex: the role of intrinsic factors. Dev Biol 2003;257:221–232. [PubMed: 12729554]

Jones EG, Hendry SHC. Co-localization of GABA and neuropeptides in neocortical neurons. Trends Neurosci 1986;9:71–76.

Kantor L, Keikilan Hewlett GH, Park YH, Richardson-Burns SM, Mellon MJ, Gnegy ME. Protein kinase C and intracellular calcium are required for amphetamine-mediated dopamine release via the norepinephrine transporter in undifferentiated PC12 cells. J Pharmacol Exp Ther 2001;297:1016–1024. [PubMed: 11356924]

Kawaguchi Y, Kondo S. Parvalbumin, somatostatin and cholecystokinin as chemical markers for specific GABAergic interneuron types in the rat frontal cortex. J Neurocytol 2002;31:277–287. [PubMed: 12815247]

Kimura F. Cholinergic modulation of cortical function: a hypothetical role in shifting the dynamics in cortical network. Neurosci Res 2000;38:19–26. [PubMed: 10997574]

Kosaka T, Kosaka K, Heizman CW, Nagatsu I, Wu J, Yanaihara N, Hama K. An aspect of the organization of the GABAergic system in the rat main olfactory bulb: laminar distribution of immunohistochemically defined subpopulations of GABAergic neurons. Brain Res 1987;411:373–378. [PubMed: 2886184]

Kosaka K, Aika Y, Toida K, Heizman CW, Hunziker W, Jacobowitz DM, Nagatsu I, Streit P, Visser TJ, Kosaka T. Chemically defined neuron groups and their subpopulations in the glomerular layer of the rat main olfactory bulb. Neurosci Res 1995;23:73–88. [PubMed: 7501303]

Kubota Y, Jones EG. Co-localization of two calcium binding proteins in GABA cells of rat piriform cortex. Brain Res 1993;600:339–344. [PubMed: 8435756]

Kubota Y, Hattori R, Yui Y. Three distinct subpopulations of GABAergic neurons in reat frontal agranular cortex. Brain Res 1994;649:159–173. [PubMed: 7525007]

Lohman AHM. The anterior olfactory lobe of the guinea pig: a descriptive and experimental anatomical study. Acta Anat 1963;53(Suppl 49):1–109. [PubMed: 14042441]

Luskin MB, Price JL. The topographic organization of the associational fibers of the olfactory system in the rat, including centrifugal fibers to the olfactory bulb. J Comp Neurol 1983;216:264–291. [PubMed: 6306065]

McDonald AJ, Mascagni F. Colocalization of calcium-binding proteins and GABA in neurons of the rat basolateral amygdala. Neuroscience 2001;105:681–693. [PubMed: 11516833]

Mundorf ML, Joseph JD, Austin CM, Caron MG, Wightman RM. Catecholamine release and uptake in the mouse prefrontal cortex. J Neurochem 2001;79:130–142. [PubMed: 11595765]

Neville, KR.; Haberly, LB. The synaptic organization of the brain. 5th ed.. Oxford University Press; New York: 2004. Olfactory cortex; p. 415-454.

Ohm TG, Muller H, Braak E. Calbindin-D-28k-like immunoreactive structures in the olfactory bulb and anterior olfactory nucleus of the human adult: distribution and cell typology-partial complementarity with parvalbumin. Neuroscience 1991;42:823–840. [PubMed: 1956518]

Schroeter S, Levey AI, Blakely RD. Polarized expression of the antidepressant-sensitive serotonin transporter in epinephrine-synthesizing chromaffin cells of the rat adrenal gland. Mol Cell Neurosci 1997;9:170–184. [PubMed: 9245500]

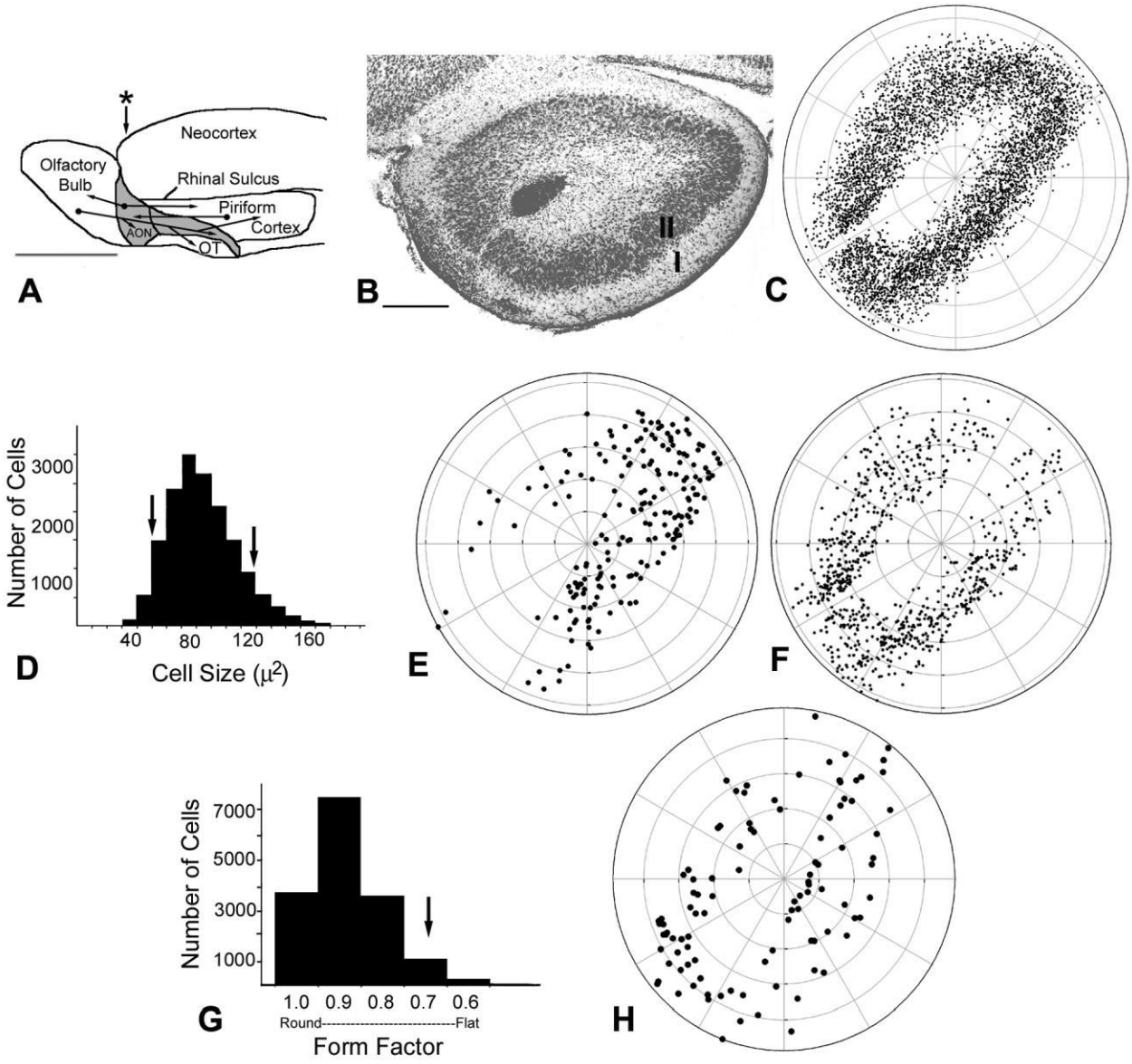

Fig. 1.

Cytoarchitectural studies of the AON. **A:** Schematic lateral view of the rat brain. The AON lies between the olfactory bulb and piriform cortex, and has heavy reciprocal connections with both structures (arrows) as well as other areas not shown. Asterisk shows approximate level of coronal section shown in B. OT, olfactory tubercle; lateral olfactory tract (LOT) shown in gray. **B:** Coronal section of the *pars principalis* region of the AON. Note the cell-free gap between the medial and ventral portions of the AON. I = superficial plexiform layer, II = deep cellular zone. **C:** Polar plot showing locations of all Nissl-stained cells from matched anterior sections of *pars principalis* from three animals. The cell-free gap in the medial portion of Layer II is a distinct boundary used as a landmark for comparisons among sections. **D:** A frequency histogram of cell size within *pars principalis* yields a unimodal distribution with a mean of 84.75 μm^2. However, when cells lying at the ends of the distribution are plotted (thresholded at arrows; 1 SD below and 2 SD above the mean), a differential pattern emerges. Large cells (>2 SD above mean soma area, panel **E**) are preferentially located in dorsolateral regions while,

small cells (cell size >1 SD below the mean, panel **F**) are more numerous in ventromedial regions. **G:** A frequency histogram of cell shape (ratio of long to short axis) within *pars principalis* suggests a uniform population of primarily round cells. **H:** A plot of relatively flat cells (ratio <0.70; arrow) reveals no regional differences in distribution of these cells. Scale bars = 5 mm in A; 300 μm in B.

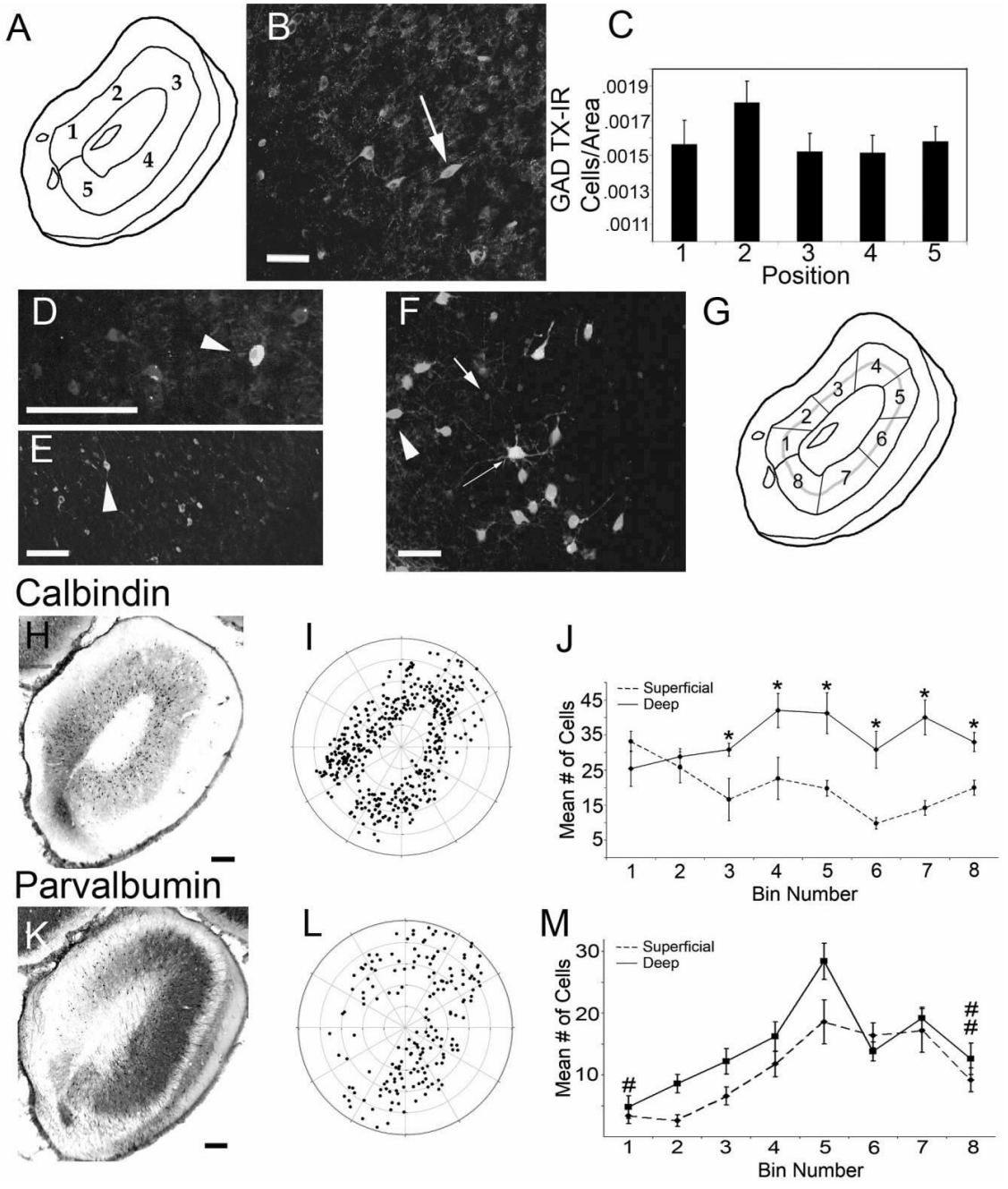

Fig. 2.

Chemoarchitectural analyses of cells in the AON. **A:** Test points used for quantification. Measurements were obtained from a 100 × 300 μm area (width by depth) for tissue immunostained for glutamic acid decarboxylase (GAD), serotonin transporter (SERT), choline transporter (CHT), and norepinephrine transporter (NET). **B:** Photomicrograph of GAD-immunoreactive (GAD-ir) cell bodies (arrow). **C:** Graph of cell counts by location in A: no regional differences in the number of GAD-ir cell bodies were observed. **D:** Photomicrograph of tissue double-labeled for GAD and parvalbumin (PARV). All PARV-ir cells double-stained for GAD (arrowhead). **E:** Photomicrograph of tissue double-labeled for calbindin (CALB) and GAD. Again, the AON contains many double-labeled cells (arrowhead), and all CALB-ir cells

double-stained for GAD. **F:** Photomicrograph of tissue double-labeled for CALB and PARV. Note that CALB (red), PARV (green), and double-labeled cells (yellow) are all visible within the AON. **G:** Parcellation of *pars principalis* used for cell counts: Layer II was divided into eight radial bins, with the bins further divided into superficial and deep halves (gray dotted line). **H:** Photomicrograph of CALB-ir cells bodies in *pars principalis*. **I:** A polar plot showing the location of all CALB-ir cells shown in (H). **J:** Counts for CALB-ir cells from five animals. Note that CALB-ir cell bodies are more prevalent in the deep portion (solid line) than in the superficial portion (dashed line) of Layer II in the dorsal and lateral regions of the AON. Note that there are no regional differences in the total number of cells. $^{*}P < 0.05$ versus superficial. **K:** Photomicrograph of PARV-ir cell bodies in *pars principalis*. **L:** Polar plot showing all PARV-ir cell bodies shown in K. **M:** Counts for PARV-ir cells from five animals. Analyses of the data revealed that significantly more cells were found in the superficial half of Layer II throughout the AON. Further, there were regional differences in the total number of cells, with significantly more cells in the lateral regions (i.e., bins 4-7; see Fig. 2G) than in the medial and ventral regions (bins 1 and 8). #$P < 0.05$ versus bins 4, 5, 6, and 7; ##$P < 0.05$ versus bins 5 and 7. Scale bars = 100 μm in B,F; 200 μm in D,E; 250 μm in I,K.

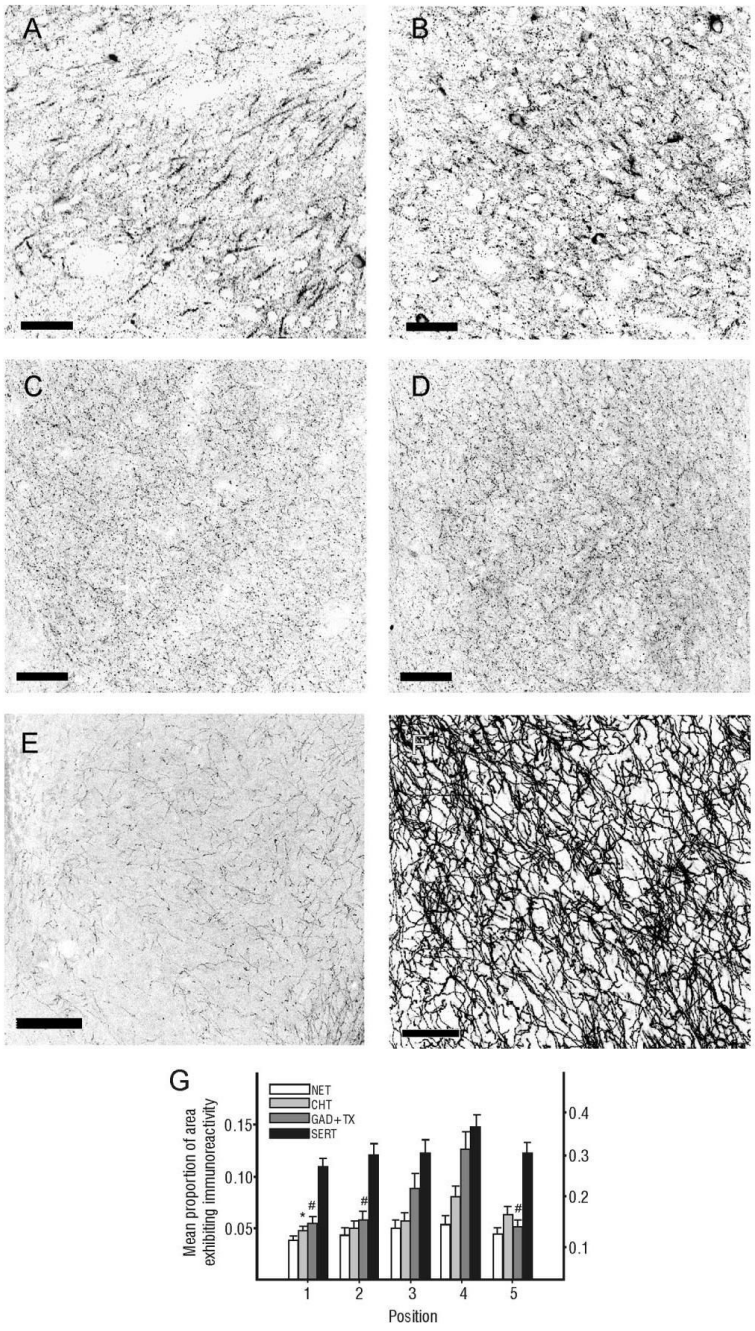

Fig. 3.

Immunohistochemical localization of neuromodulatory fiber systems. Tissue stained for this study was analyzed using the same measurement scheme depicted in Figure 2A. Analyses of GAD-ir fibers (shown for position 5 (**A**) and 4(**B**)) and of choline transporter (CHT) immunoreactive fibers (shown for position 1 (**C**) and 4(**D**)) revealed significant differences among AON regions. Tissue stained for norepinephrine transporter (NET; **E**) and serotonin transporter (SERT, **F**) revealed a similar trend in labeling density. **G:** Graph representing data for all five positions of pars principalis for GAD, CHT, NET, SERT. *,#$P < 0.05$ versus position 4. Left axis corresponds to NET and CHT data and right axis corresponds to GAD-TX and SERT data. Scale bars = 50 μm in A-D; 100 μm in E,F.

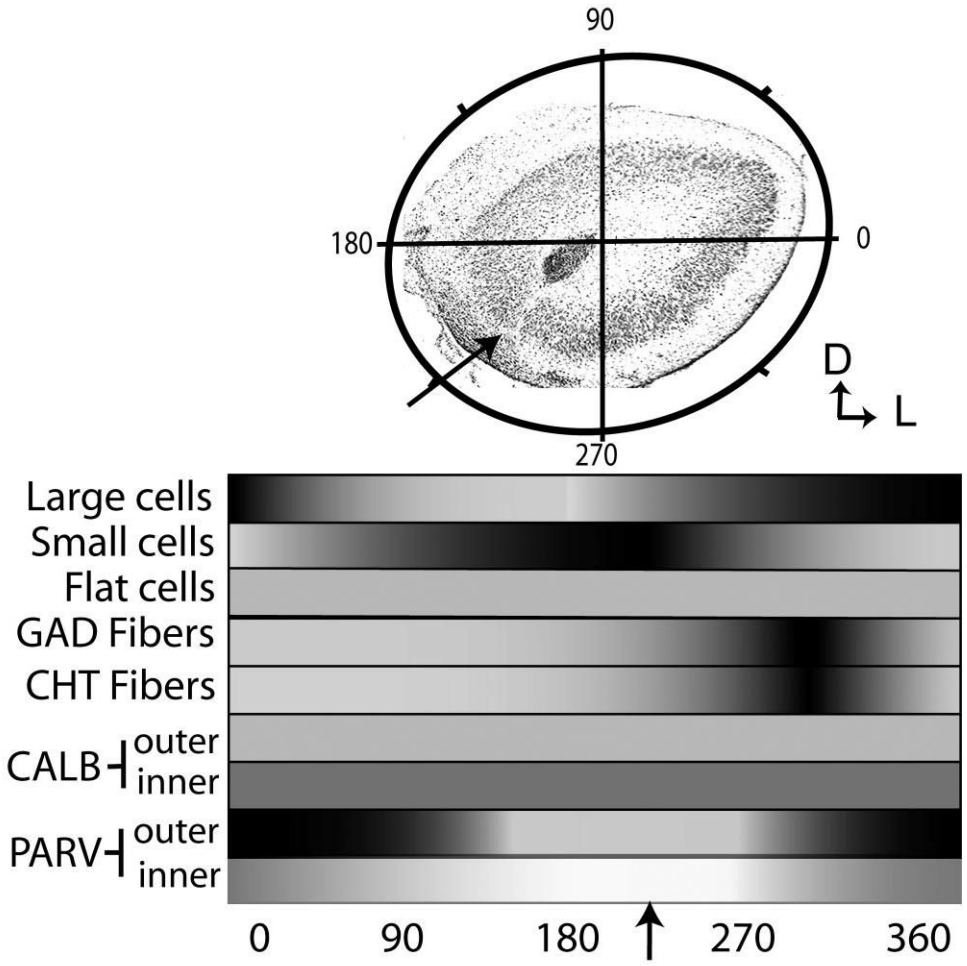

Fig. 4.

Summary of results. Top: The AON is shown with an overlay that divides the cellular region radially, with 0-180° representing the mediolateral axis. This coordinate system is used to organize the results graphically. The arrow shows the location of the cell-free zone on the ventromedial aspect of *pars principalis*. Bottom: Shading represents relative density of the various features along the radial dimension. For example, large cells (found in the highest densities in the lateral regions of the AON, see Fig. 1E) are represented by the dark band from 270° to 30°. Small cells (found primarily in ventromedial areas, see Fig. 1F) extend from ~100° to 250°.